Reflected-Shock Non-Idealities in Shock Tubes: The Impact of the Facility-Dependent Effects over a Wide Range of Pressures and Mach Numbers

D. Nativel[a], M. Fikri[a], J.T. Lipkowicz[b], A.M. Kempf [b] C. Schulz[a]
Institute for Combustion and Gas Dynamics
a) Reactive Fluids, b) Fluid Dynamics
University of Duisburg-Essen
Duisburg, Germany

S. P. Cooper, E. L. Petersen
J. Mike Walker '66 Department of Mechanical Engineering
Texas A&M University
College Station, Texas, USA

1 Introduction

Shock tubes are frequently used for studying fast chemical processes. This application requires accurate knowledge of the post-shock conditions. Ideally, the thermodynamic state behind the reflected shock wave is homogeneous and can be calculated from the initial, driven-gas conditions and the speed of the incident shock wave. However, deviations from the ideal assumption can significantly affect the system and lead to time-dependent changes in temperature and pressure. In shock tubes, non-ideal effects have an impact on the experiments and can cause deviations from ideal behavior such as uncertainties in the determination of chemical kinetic rate constants as well as premature ignition at lower temperatures.

Viscous effects lead to the development of a side-wall boundary layer behind the incident shock. This boundary layer contributes to the attenuation of the incident shock wave; other effects can also contribute, such as finite opening time of the diaphragm and finite formation time of the shock wave [1]. The reflected shock wave also propagates through the boundary layer, causing interfering waves, further shock attenuation, and variations in the thermodynamic state of the compressed test gas [2]. These disturbances cause an observable change in the form of pressure and temperature rise in the post-shock region [3]. At higher pressures, a gradual increase in pressure is observed and is included to simulate ignition values [4]. Shock-tube geometry and design contribute to these effects and impact experimental results, such as ignition delay time, for different shock tubes. To cope with these effects, largely empirical correction strategies have been developed in the past that yielded significant improvement. For example, the increase of pressure

Correspondence to: damien.nativel@uni-due.de

behind the reflected shock wave could be compensated for, to some degree, using driver inserts [5]. However, there is not a good enough understanding of the underlying effects that would lead to universally applicable strategies. These can only result from a direct coupling of experiment and simulation.

As a first step, the present work aims to develop a database to determine conditions where non-ideal gas-dynamic effects can be neglected for a given shock tube. With this aim in mind, characterization of facility effects was targeted by adopting two different laboratories (Texas A&M University, or TAMU, and the IVG at the University of Duisburg-Essen, UDE) and different regimes (variation of temperatures, Mach numbers, and pressures). The overall objective was to measure characteristic quantities related to facility-dependent effects and to develop a detailed database for simulation purposes that demonstrates, for example, the resulting impact on uncertainties in ignition delay times. Thus, pressure rise behind reflected waves (i.e., dp*/dt) were measured for a wide range of Mach numbers and pressures (~2.1–4.1 and 2–30 bar, respectively) for pure argon and pure nitrogen as driven gas.

The dp*/dt is defined as the immediate pressure rise behind the reflected wave. It is well known that the primary cause of dp*/dt stems from viscous effects associated with the propagation of the incident shock wave and subsequent boundary-layer growth, and secondarily from diaphragm-opening mechanics [3]. Therefore, to investigate correlations between experimental results and boundary-layer growth-rates behind the incident shock, the boundary-layer thickness (δ) of a wholly laminar and wholly turbulent boundary layer was numerically calculated.

In the present paper, the methodology adopted to measure dp*/dt consistently in the two different laboratories is described followed by a presentation of the experimental results and a discussion fed by boundary-layer calculations recently obtained from the in-house code.

2 Experimental Details and Data Acquisition

For each laboratory, a conventional shock tube (abbreviated AST, “Aerospace Shock Tube” and CST, “Conventional Shock Tube” for TAMU and UDE, respectively) and a high-pressure shock tube (HPST-TAMU or HPST-UDE) were chosen for the study. Each shock tube exhibits different geometries (internal diameter, ID, and length of the driven section, L_{driven}) as presented in Table 1. The four shock tubes are approximately comparable in terms of the length L_{driven} of the driven section but have noticeable differences in ID. More-detailed descriptions of the two TAMU and UDE facilities can be found elsewhere [6-9]. The pressure–time distribution in the shock tubes was measured using piezo-electric sensors. Different types of sensors were used. Two sensors (side-wall mounted at 1.6 cm from the end-wall) Kistler and PCB (model 603B1 and 113A, respectively) for TAMU and a sensor from PCB (model 112A03) for the UDE (side-wall mounted at 2.0 cm from the end-wall).

Table 1: Details of the shock tubes.

	ID / cm	L_{driven} / m
AST - TAMU	16.20	7.88
HPST - TAMU	15.24	5.03
CST - UDE	8.00	8.00
HPST - UDE	9.00	6.10

The transducers are insulated with a thin layer (~0.5 mm, based on manufacturer recommendations) of RTV silicone to minimize heat transfer effects. The post-reflected-shock pressure rise, or dp*/dt (=(dp_5/p_5)/dt in %/ms), was measured following the procedure explained by Hargis and Petersen [3]. A linear fit (orange lines in Fig. 1) was made over the first 2 ms after the shock, where the pressure trace evolves in an almost

linear manner. Special care was taken in this calculation to be consistent between the two laboratories. An example pressure trace and dp*/dt determination are given in Fig. 1 for each laboratory.

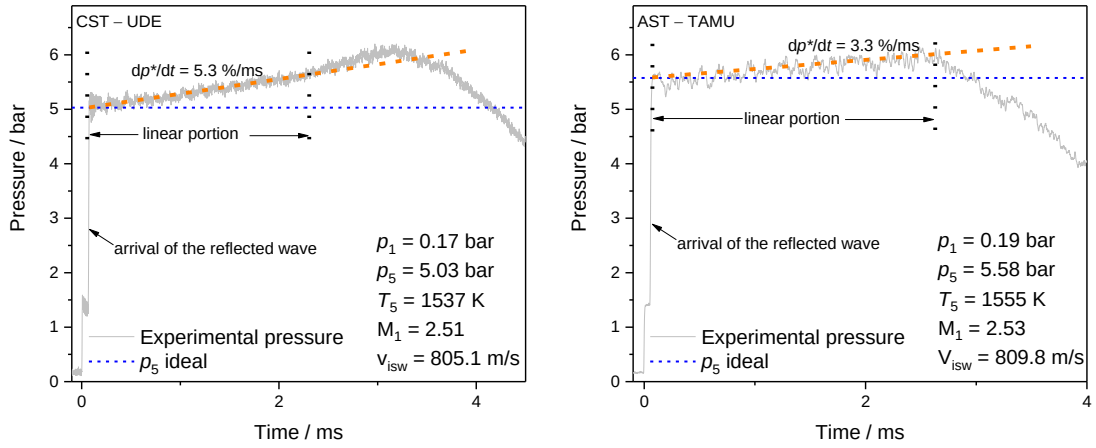

Figure 1. Typical side-wall pressure traces of dp*/dt in Ar. Left: UDE laboratory; right: TAMU laboratory.

3 Results and Discussion

The post-reflected-shock pressure rise (dp*/dt) data were taken for test pressures (p_5) between 2 and 30 bar for incident-shock Mach numbers between 2.1 and 3.1 for Ar, and between 2.1 and 4.1 for N_2. All the data shown in Fig. 2 were obtained using He as the driver gas. We observed a strong dependence of dp*/dt on the Mach number for both series of experiments (Ar or N_2). Strong scatter is observed on each individual set of data, which is due to test-to-test variations (diaphragm bursting mechanics, finite opening time of the diaphragm, etc.).

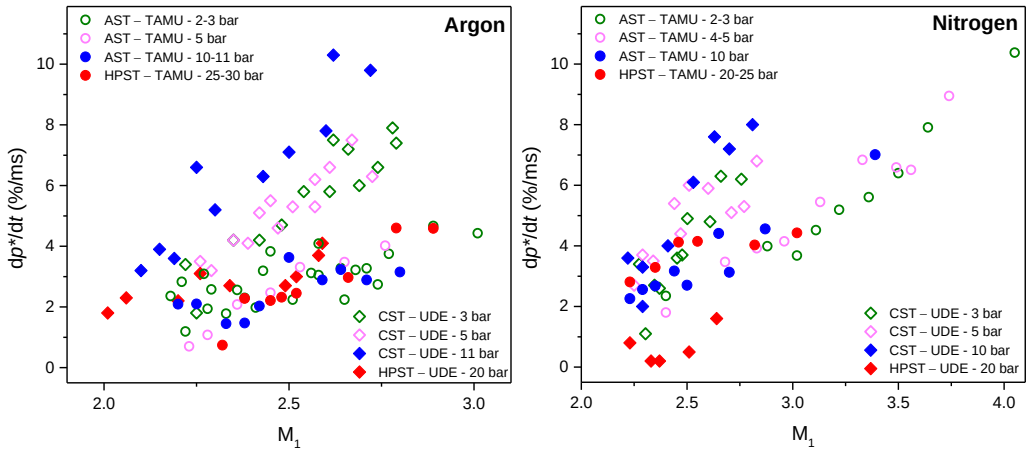

Figure 2. Evolution of the dp*/dt with incident-shock Mach number, M_1 at different pressures for pure Ar (left) and pure N_2 (right).

For the argon data, the dp*/dt is larger for the UDE shock tubes than for the TAMU shock tubes at the same Mach number except for the high-pressure data where the difference is less noticeable. Looking at just the AST and CST data (p_5 up to 10 bar), there is a difference of about a factor of two between the two facilities.

For the N_2 data, three trends are observed. First, the CST – UDE data exhibit larger dp*/dt compared to the AST and HPST from TAMU. The dp*/dt data from HPST – UDE are much lower than the others, with dp*/dt < 2%/ms. We can attribute these variations on the differences in shock-tube geometry considering the differences between the data from large- and small-diameter shock tubes. On the other hand, especially for the N_2 data, we surprisingly observed a much lower dp*/dt, presuming additional factors that are not considered in this study.

The idea of this work was to acquire a solid database in terms of facility-dependent effects on reflected-shock conditions over multiple devices. Therefore, from the entire set of experimental data, a general correlation taking into account the varied parameters was obtained. This correlation is presented in Fig. 3.

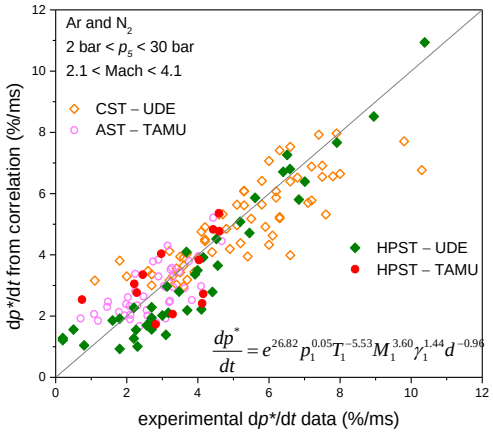

Figure 3. Data from the dp*/dt correlation plotted against experimental measured dp*/dt.

The dp*/dt data were correlated to the incident-shock Mach number M_1, the initial pressure in the driven section p_1, the specific heat ratio of the driven gas prior to arrival of the incident shock wave γ_1, the initial temperature T_1, and the diameter of the driven section d. This last parameter was chosen to take into account the facility geometry dependence. T_1 was also chosen since the temperature of HPST – UDE was 323 K and for HPST – TAMU, 295 K (T1 was also nearly 295 K for the AST and the CST). Overall, each parameter helped to ameliorate the correlation, but their inclusion needs further investigation, such as a sensitivity analysis.

A comparison between measured dp*/dt and the boundary layer-growth rate dδ/dt is shown in Fig. 4. As explained by Hargis and Petersen [3], the boundary layer generates disturbances largely responsible for the occurrence of dp*/dt. To calculate the boundary-layer thickness, an in-house code was developed. The state behind the incident shock wave is computed using the common shock relations, as presented by Mark [10]. Single-species gas properties were pre-tabulated as a function of temperature, while the mixture-averaged properties were calculated over the run time. The analytical solution from Mirels [11] was applied to derive a wholly laminar solution for the given state behind the incident shock. The system of ordinary differential equations was integrated utilizing a four-step Runge-Kutta scheme. Since the initial values of the ordinary differential equations are not completely known, an iterative shooting method was used. To derive a solution of a wholly turbulent boundary layer, an integral method of Mirels [11] was used assuming that the axial velocity within the boundary layer is related to the free stream velocity by a 7th power law. The authors chose in a similar way as Hargis and Petersen [3] to simplify the interpretation of the boundary-layer profiles assuming an immediate turbulent boundary layer behind the incident shock wave. To have an easier

comparison between the measured dp*/dt and the calculated dδ/dt, the turbulent boundary layer was linearized, and the slope of the linearized profile was taken as a form of boundary-layer growth rate, dδ/dt in mm/ms.

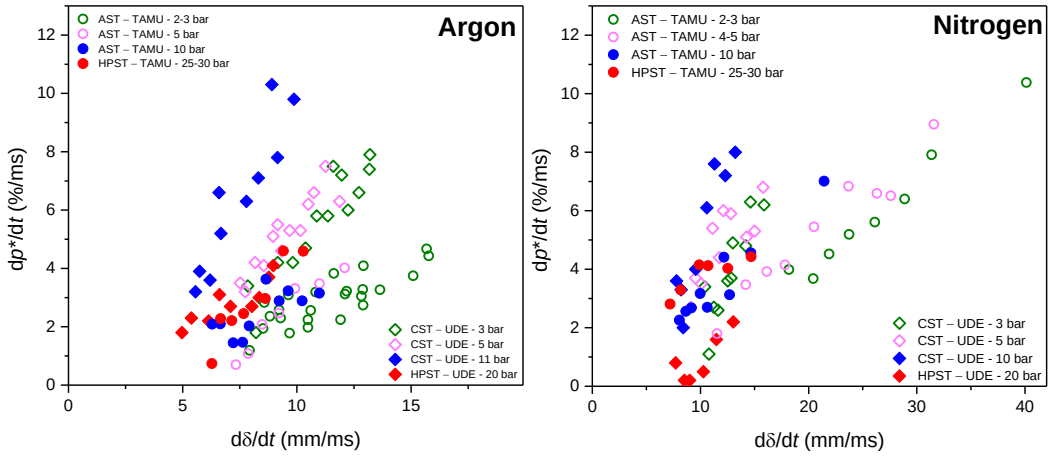

Figure 4. Evolution of the dp*/dt with the boundary-layer growth rate at different pressures. Left: Ar; right: N_2.

For the same range of pressure and for a fixed dδ/dt, a higher dp*/dt for the CST and HPST from UDE is observed. This larger pressure increase is expected for the smaller-diameter tubes because for the same shock conditions the boundary layer occupies a larger percentage of the tube's cross-section. Therefore, it was not unexpected to have higher dp*/dt for the smaller-diameter shock tubes. It should be noted that the experiments at higher Mach number for N_2 at TAMU (Fig. 4) should not be considered as a facility-dependent effect due to the lack of similar experiments at UDE. Finally, very low dp*/dt values are observed with HPST – UDE with N_2. Nevertheless, this observation needs further investigation since the dδ/dt data are comparable to those from the TAMU – HPST. This result is not consistent with the theoretical behavior since HPST – TAMU has a much larger inner diameter than HPST – UDE.

4 Conclusions and Future Work

The post-shock pressure rise (i.e., dp*/dt) was measured for a wide range of Mach numbers and pressures (~2.1–4.1 and 2–30 bar, respectively) for argon and nitrogen in four shock tubes with different geometry. A strong Mach number dependence was noticed, and also a clear dependence on the shock-tube geometry from these data considering the differences between the data from large and small diameter shock tube was found. We observed the lowest dp*/dt at around 20 bar in HPST – UDE, but this needs further investigation to understand the difference compared to the HPST – TAMU. A correlation was established to help rationalize facility-dependent effects for the shock tubes.

Further work is needed to understand the correlation using a sensitivity analysis. The dp*/dt versus boundary-layer-growth rate could be correlated since the boundary-layer model incorporates all of the properties of interest such as pressure, temperature, and M_1.

5 Acknowledgments

This work was supported by the German Research Foundation within the DFG Project SCHU 1369/27 and KE 1715/8. Additional support came from the TEES Turbomachinery Laboratory.

References

[1] Davidson DF and Hanson RK. (2009). Recent advances in shock tube/laser diagnostic methods for improved chemical kinetics measurements. Shock Waves 19: 271.

[2] Mirels H. (1972). Boundary layer growth effects in shock tubes. Proc. 8th Int. Shock Wave Symp. 2-30.

[3] Hargis JW and Petersen EL. (2017). Shock-tube boundary-layer effects on reflected shock conditions with and without CO_2. AIAA journal. 55: 902.

[4] Pang GA, Davidson DF, Hanson RK. (2009). Experimental study and modeling of shock tube ignition delay times for hydrogen–oxygen–argon mixtures at low temperatures. Proc. Combust. Inst. 32: 181.

[5] Hong Z, Pang GA, Vasu S, Davidson DF, Hanson RK. (2009). The use of driver inserts to reduce non-ideal pressure variations behind reflected shock waves. Shock Waves. 19: 113.

[6] Vivanco JE (2014). A New Shock-Tube Facility for the Study of High-Temperature Chemical Kinetics (Master's Thesis), Texas A&M University, College Station, TX.

[7] Aul CJE (2009). An Experimental Study into the Ignition of Methane and Ethane Blends in a New Shock-Tube Facility (Master's Thesis), Texas A&M University, College Station, TX.

[8] Zabeti S, Fikri M, Schulz C. (2017). Reaction-time-resolved measurements of laser-induced fluorescence in a shock tube with a single laser pulse. Rev. Sci. Inst. 88: 115105.

[9] D. Nativel et al., Shock-tube study of methane pyrolysis in the context of energy-storage processes, Proceedings of the Combustion Institute (2019), https://doi.org/10.1016/j.proci.2018.06.083.

[10] Mark H. (1958). The Interaction of a Reflected Shock Wave with the Boundary Layer in a Shock Tube. NACA TM 1418.

[11] Mirels H. (1956). Boundary layer behind shock or thin expansion wave moving into stationary fluid. NASA Techn. Note 3712.